Available online www.jsaer.com

Journal of Scientific and Engineering Research, 2018, 5(7):259-269

Research Article

ISSN: 2394-2630
CODEN(USA): JSERBR

3D Study of a Silicon Solar Cell under Constant Monochromatic Illumination: Influence of Both, Temperature and Magnetic Field

Attoumane Mamadou Moustapha KOSSO[1], Moustapha THIAME[2], Youssou TRAORE[3], Ibrahima DIATTA[3], MorNDIAYE[3], Lemrabott Habiboullah[4], Ibrahima LY[5], Grégoire SISSOKO[2]

[1]Ecole des mines et de la géologie de Niamey- Niger.
[2]Departement de physique- Laboratoire LCPN-Université Assane SECK-Ziguinchor-Sénégal
[3]Laboratoire des Semi-conducteurs et d'Energie Solaire, Faculté des Sciences et Techniques, Université Cheikh Anta Diop, Dakar, Sénégal
[4]Ecole Supérieure Polytechnique de Nouakchott- Mauritanie
[5]Ecole Polytechnique de Thiès, Sénégal

Abstract In this work, we deal with a three-dimensional modeling study of a silicon solar cell in steady state, at the temperature **T**, under monochromatic illumination of wavelength **λ** and placed in a magnetic field **B**. The use of the maximum diffusion law as a function of the optimal temperature made it possible to choose the values of the magnetic field **B** in the study of the effective diffusion coefficient $\mathbf{D_{k,j}}$. The effect of both, the magnetic field **B** and the temperature **T** on the excess minority carrier density $\boldsymbol{\delta(x, y, z)}$ is analyzed through the determination of the eigenvalues ($\mathbf{C_k}$, $\mathbf{C_j}$), for different grain sizes ($\mathbf{g_x}$, $\mathbf{g_y}$) and there combination velocity at the grain boundaries $\mathbf{S_g}$.

Keywords Silicon solar cell -Magnetic field-Temperature- grain size and recombination velocity-Eigenvalues

1. Introduction

The performance of a solar cell, used for photovoltaic conversion, depends on several parameters including the nature and structure of the semiconductor, its manufacturing technique and the operating conditions [1-3]. Thus, in order to improve the efficiency, different techniques using the silicon solar cell (monofacial, bifacial [4- 6], vertical Multijunction [7-8]) at 1D orat 3D [9-15] were developed. These techniques use static regimes [16], dynamic frequency regime [17-19] and transient [20-23]. Among the most commonly used characterization techniques, are those with constant or pulsed external signal as, optical excitation(mono orpolychromatic), electrical excitation (E, electron).The experimental conditionskeep the solar cell under:

a) sun concentration (n), and variableangle of incidence θ [24, 25]
b) Temperature T [26]
c) Magnetic field B [27,28]
d) Irradiation with Φp the flux and, K_l the intensity of irradiation with nuclear particles [29].

The results are analyzed by use of physicphenomenological parameters i.e., excess minority carrier diffusion coefficient (D), lifetime (τ), diffusion length (L), recombination velocities at the junction Sf, at the rear (Sb) and at the grain surface (Sg) [11].

The physicmacroscopic parameters are takenfrom electrical equivalent model i.e.: short circuit current density (Jsc), open circuit voltage (Voc), maximum current density (Jmax), maximum photovoltage (Vmax), fill factor

(FF), efficiency (η), series and shunt resistances (Rs, Rsh), transitional and diffusion capacitance (Cz), impedance (Z), cut off frequency (ωc), self-inductance (Lh) [30,31].

This study combines the parameters of temperature T and magnetic field B, for a static operation of the solar cell under monochromatic illumination (short wavelength), taking into account grain size and grainrecombination velocity at boundaries. Then new eigenvalues are obtained from new excess minority diffusion coefficient D * (B, T). Thus the excess minority carrier can be studied.

2. Theoretical Study

2.1. Description of the Silicon Solar Cell

The polycrystalline substrate is composed of several grains or crystallites of any shape and size. For a three-dimensional modeling study, we will use the columnar model where each grain is assumed to have a regular parallelepipedal shape [11, 32-35] (Figure 1).

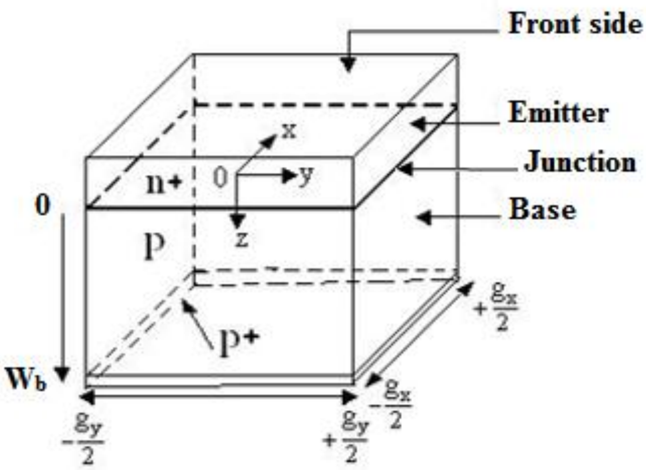

Figure 1: The columnar geometry of a grain used in the model, with $\vec{B} = B.\vec{\imath}$

The silicon solar cell on which our study will focus is monofacial typen$^+$-p-p$^+$ (figure 1 c). The silicon solar cell is trained of four major essential parts:

The emitter (type n), heavily doped zone (10^{17} - 10^{19} cm^{-3} phosphorus atoms), is called the front face of the solar The thickness of the emitter is of the order 0.3 at 1 µm.

The base (type p), with thickness (100 - 400 µm), is weakly doped (from 10^{15} to 10^{17} cm^{-3} boron atoms).

The emitter and the base are separated by a zone without charge called space charge region(SCR) where a strong electric field prevails,called the junction.

The back surface (type p$^+$) consisting of an area on endowed with impurities (from 10^{17} to 10^{19} cm^{-3}) where is an electric field, that allows the photogeneratedcarrier to reach the junction.

2.2. Steady state continuity equation of the density of charge carrier

In a semiconductor the concentration of minority carrier will be greater in the illuminated region than in the semiconductor remainder. There is a concentration gradient in the semiconductor. There is a phenomenon of diffusion of the minority carrier of the region of high concentration towards the region of low concentration. This diffusion process obeys the first law of Fick [11]:

$$J = -eD\frac{\partial\delta}{\partial x} = -eD\overrightarrow{grad}(\delta) \qquad (1)$$

J is the current density due to the minority carrier;

Δ is the density of minority carrier;

D represents the diffusion coefficient that depends on the nature of the semiconductor and µ characterizes the mobility of electrons by the Einstein's relation:

$$\frac{D}{\mu} = \frac{kT}{e} \qquad (2)$$

e =1.610^{-19} c, is the elementary charge, T is the temperature and k the Boltzmann constant (k= 8.62 10^{-5} eV/°K)

In the three-dimensional case where the semiconductor grain is represented by Figure 1; the continuity equation which governs the excess minority carrier density in the base, is written as **[**15, 35, 36**]**:

$$D\left[\frac{\partial^2\delta(x,y,z)}{\partial x^2}+\frac{\partial^2\delta(x,y,z)}{\partial y^2}+\frac{\partial^2\delta(x,y,z)}{\partial z^2}\right]-\frac{\delta(x,y,z)}{\tau}+g(z)=0 \quad (3)$$

with: δ(x,y,z) represents the excess minority carrier density in the base g(z) represents the generation rate of the minority carrier which depends on z, depth in the base according to the fallowing relation:

$$g(z)=\alpha(\lambda)[1-R(\lambda)]I_0e^{-\alpha(\lambda)z} \quad (4)$$

$\alpha(\lambda)$ is the monochromatic optical absorption coefficient at the wavelength λ,

$R(\lambda)$ is the reflection coefficient of the material at the wavelength λ,

I_0 is the incident illumination flux.

τ is the electron lifetime in the base.

The solar cell undermagnetic field B, the coefficient and diffusion length of excess minority carrier change with the relation [37, 38, 39]:

$$D^*=\frac{D}{1+(\mu B)^2} \quad et \quad L^*=\sqrt{\tau D^*} \quad (5)$$

The equation (3) becomes:

$$\left[\frac{\partial^2\delta(x,y,z)}{\partial x^2}+\frac{\partial^2\delta(x,y,z)}{\partial y^2}+\frac{\partial^2\delta(x,y,z)}{\partial z^2}\right]+\frac{g(z)}{D^*}=\frac{\delta(x,y,z)}{\tau D^*} \quad (6)$$

$$\frac{\delta(x,y,z)}{\tau D^*}=\Delta\delta(x,y,z)+\frac{g(z)}{D^*} \quad (7)$$

$$With \qquad D^*\tau=L^{*2}$$

$$\frac{\delta(x,y,z)}{L^{*2}}=\Delta\delta(x,y,z)+\frac{g(z)}{D^*} \quad (8)$$

The general solution of the continuity equation (8) can be expressed as:

$$\delta(x,y,z)=\sum_k\sum_j F_{kj}(z)\cos C_k x\cos C_j y \quad (9)$$

$F_{kj}(z)$ represents the spatial function of the density of excess minority carrier depending on the base depth z. The C_k and C_j are the eigenvalues obtained using the following boundary conditions at the grain boundaries.

$$\frac{\partial}{\partial x}\delta(x,y,z)\Big]_{x=\pm\frac{g_x}{2}}=\pm\frac{S_g}{D^*}\delta\left(\pm\frac{g_x}{2},y,z\right) \quad (10)$$

$$\frac{\partial}{\partial y}\delta(x,y,z)\Big]_{y=\pm\frac{g_y}{2}}=\pm\frac{S_g}{D^*}\delta\left(x,\pm\frac{g_y}{2},z\right) \quad (11)$$

S_g is the excess minority recombination velocity at grain boundaries. The eigenvalues C_k and C_j are determinate by transcendental equations expressed as:

$$\tan C_k\frac{g_x}{2}=\frac{S_g}{C_kD^*} \quad (12)$$

$$\tan C_j\frac{g_y}{2}=\frac{S_g}{C_jD^*} \quad (13)$$

The solutions of equations (12), (13) is obtained by a graphic resolution [40] instead of numerical one.

Using the orthogonality of $\cos(C_k.x)$ and $\cos(C_jy)$ functions, we obtain the $F_{k,j}(z)$ expression as:

$$F_{kj}(z)=A_{kj}\cosh\left(\frac{z}{L_{kj}}\right)+B_{kj}\sinh\left(\frac{z}{L_{kj}}\right)-\frac{\alpha I_0(1-R)L_{kj}^2}{D_{kj}\left(\alpha^2L_{kj}^2-1\right)}e^{-\alpha z} \quad (14)$$

With L_{kj} the effective diffusion length expressed as

$$\frac{1}{L_{kj}^2}=C_k^2+C_j^2+\frac{1}{L^{*2}} \quad (15)$$

And D_{kj}, the effective diffusion coefficient

$$D_{kj}=\frac{D^*[g_xC_k+\sin(C_kg_x)].[g_yC_j+\sin(C_jg_y)].}{16.\sin\left(C_k\frac{g_x}{2}\right).\sin\left(C_j\frac{g_y}{2}\right)} \quad (16)$$

The constants A_{kj}, and B_{kj} are obtained with the boundary conditions at the junction and back surfaces:

$$D^*\frac{\partial}{\partial z}\delta(x,y,z)=S_f\delta(x,y,z) \quad for \quad z=0 \quad (17)$$

$$D^*\frac{\partial}{\partial z}\delta(x,y,z)=-S_b\delta(x,y,z) \quad for \quad z=H \quad (18)$$

In these expressions, Sf represents the excess minority carrier recombination velocity at the junction which accelerated the flow of carrier crossing the junction and Sb is the recombination velocity on the back surface and reflected the minority carrier toward the junction(back surface field) [41-43].

2.3. Diffusion Coefficient

The diffusion coefficient D * (B, T) of the minority carrier in the base under influence of temperature T and the applied magnetic field B is obtained by the relation [28, 44]:

$$D^*(B,T) = \frac{D(T)}{1+(\mu(T)B)^2} \tag{19}$$

With$D(T) = \mu(T)\frac{KT}{q}$ (20)

and

$$\mu(T) = 1{,}43.10^9 T^{-2.42} cm^2 v^{-1} s^{-1} \tag{21}$$

The Umklap's process, is justified, that for a given value of the magnetic field, the optimum temperature is obtained when the diffusion coefficient reaches its maximum. Using the graphical and analytical methods, the optimal temperature as a function of the magnetic field [44] can be given by the following relation:

$$T_{op}(B) = \sqrt[4,85]{5{,}2349.10^{18}B^2} = \sqrt[4,85]{2{,}56(1{,}43.10^9)^2.B^2} \tag{22}$$

This relation allows us to optimize the diffusion coefficient in the determination of eigenvalues Ck and Cj, through transcendental equations.

2.4. Eigenvalues C_k et C_j determination:

The coefficients C_k et C_j are space eigenvalues obtained through transcendental equations (23) and (24) either graphically.

We have opted for the graphical method, where by plotting the functions f (Ck) and h (Ck) below, the points of intersection of the two curves yield, the Ck. The Cj are obtained in the same way. Keeping gx = gy the Ck and Cj have the same values.

$$f(C_k) = \tan C_k \frac{g_x}{2} \tag{23}$$

$$h(C_k) = \frac{1}{C_k} \times \frac{S_g}{2D^*} \tag{24}$$

We notice that for $S_g \leq 10^3$ cm.s^{-1}, C_k (or C_j) values seem to be insensitive to both the variations of the magnetic field and Sg. In the table (1) we have noted the values obtained from Figures 2a and 2b.

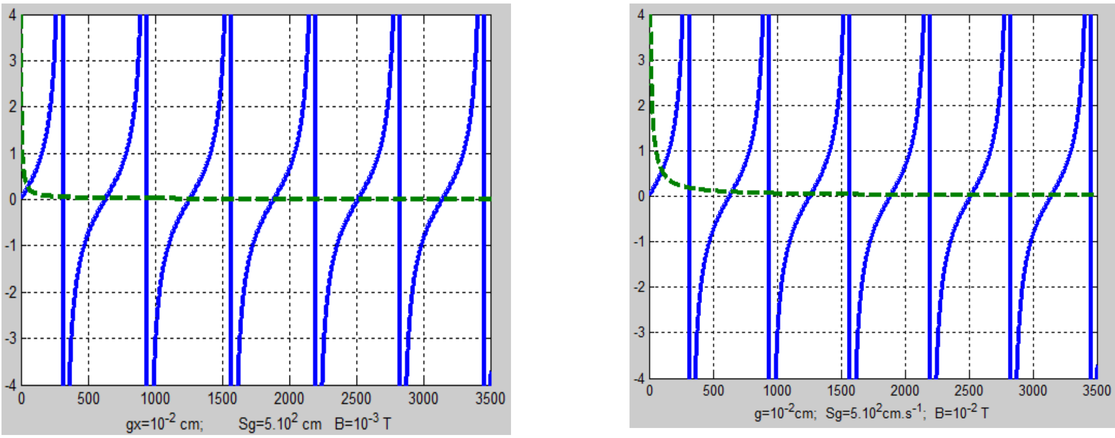

(a) *(b)*

Figure 2: eigenvalue for $s_q \leq 10^3$ cm.s^{-1} ; B=10^{-2} T et B=10^{-3} T

The table 1 gives the eigenvalues C_k for $s_g \leq 10^3$ cm.s^{-1}

Table 1: eigenvalues C_k for $s_g \leq 10^3$ cm.s^{-1}

Magnetic field B [T]	Eigen value C_k (cm^{-1})				
10^{-2}	630	1255	1887	2516	3144
10^{-3}	630	1255	1887	2516	3144

We verified for several recombination velocity at grain boundaries sg ≤ 10^3 cm.s^{-1} and for different values of the magnetic field; the C_k (or C_j) valuesare substantially equal to the values given in Table 1 (Low manifestation of the Lorentz forces).
For 10^3 cm.s^{-1}<Sg <10^5 cm.s^{-1} the C_k (or C_j) values vary and increase as the magnetic field increases (Figs. 3a and 3b) as indicated by the founded values in Table 1.

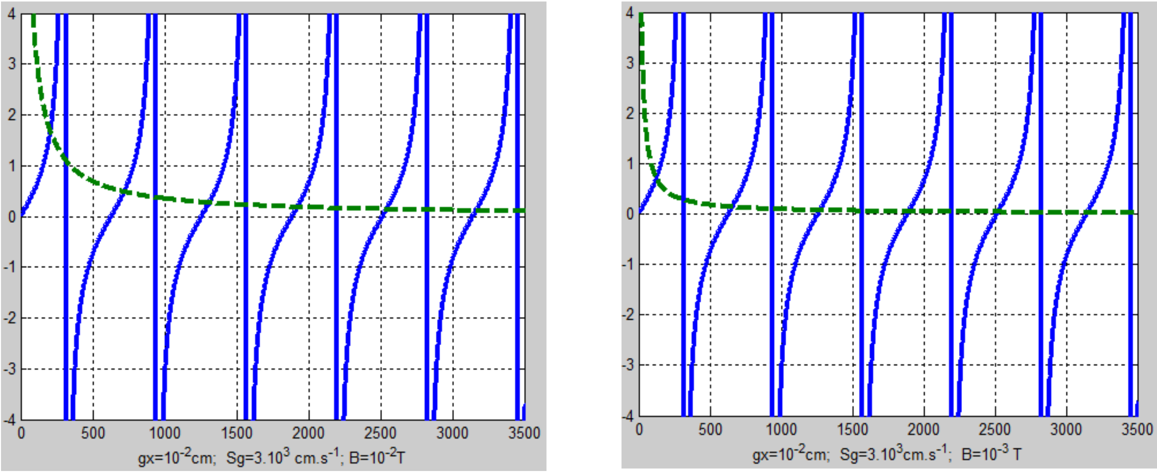

(a) (b)

Figure 3: eigenvalues for10^3 cm.s^{-1} < S_g < 10^5 cm.s^{-1}; B=10^{-2} T et B=10^{-3} T

The table 2 gives the eigenvalues C_k for S_g= 3.10^3 cm.s^{-1}

Table 2: eigenvalue C_k for S_g= 3.10^3 cm.s^{-1}

Magnetic field B [T]	Eigenvalue C_k				
10^{-2}	719	1307	1920	2542	3164
10^{-3}	660	1269	1897	2526	3148

When Sg> 10^5 cm.s^{-1} the values of C_k (or C_j) become very sensitive to the variations of the magnetic field; in figure 4 gives these values for B = 10^{-5} T and B = 10^{-4} T with a value of Sg = 5. 10^5 cm.s^{-1}. (Strong manifestation of the Lorentz forces, for large B and Sg values).

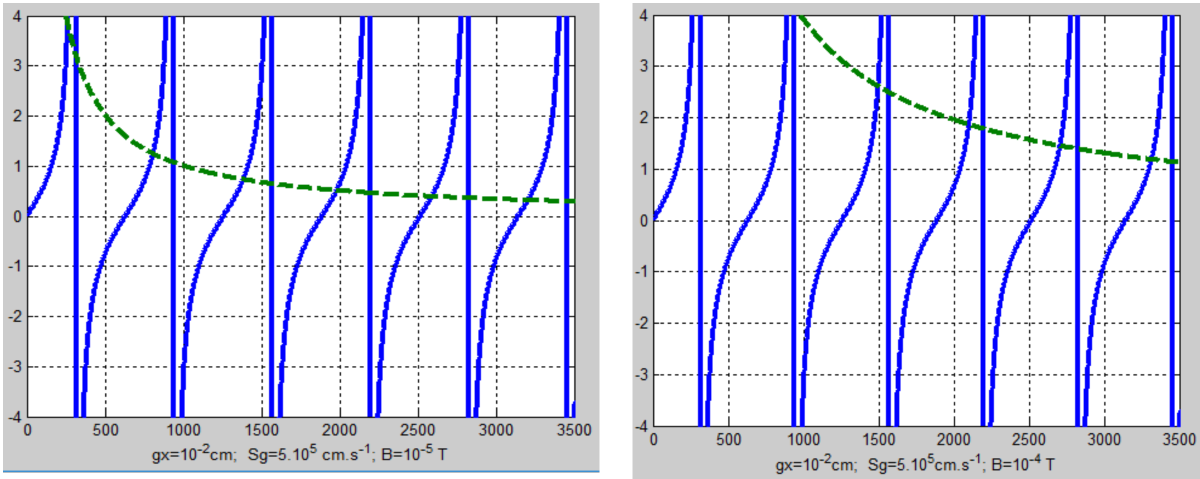

(a) *(b)*

Figure 4: egenvalues s_g>10^5 cm.s^{-1} ; B=10^{-2} T et B=10^{-3} T

The table 3 offers the eigenvalues C_k for S_g= 5.10^5 cm.s^{-1}

Table 3: eigenvalues C_k for S_g = 5.10^5 cm.s^{-1}

Magnetic field B [T]	Eigenvalues C_k				
10^{-5}	809	1384	1983	2592	3204
10^{-4}	1496	2101	2707	3319	

Also, the grain size gx has a very large influence on the eigenvalues, irrespective of the recombination velocity at the grain boundaries and the magnetic field; all previous curves were plotted for gx = 10^{-2} cm.

For the curve below (figure 5) we took gx = 2.10^{-2} cm; we note that for the same interval the number of eigenvalues Ck has practically doubled, according to equation (12).

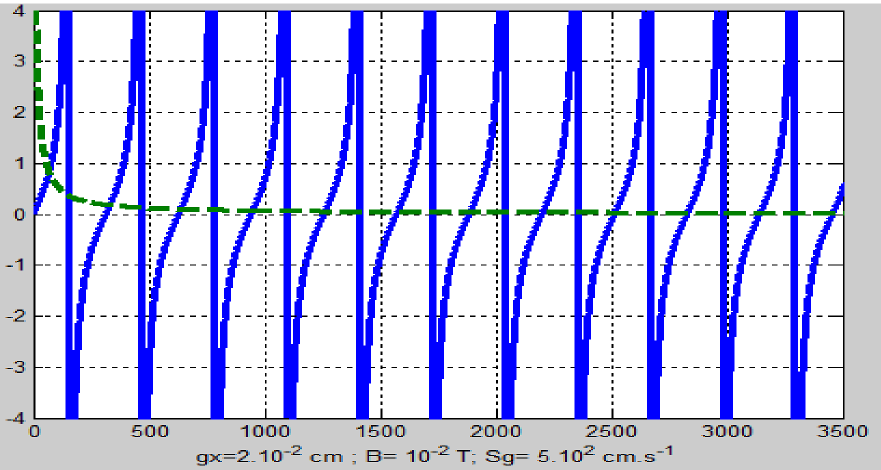

Figure 5: eigenvalues s_g=5.10^2 cm.s^{-1}; B=10^{-2} T

2.5. Excess minority carrier density in the base

δ(x,y,z) represents the density of excess minority charge carrier in the base, its expression is given by the resolution of equation (25):

$$\delta(x,y,z) = \sum_k \sum_j [A_{kj} \cosh(\frac{z}{L_{kj}}) + B_{kj} \sinh(\frac{z}{L_{kj}}) - \frac{\alpha I_0(1-R)L_{kj}^2}{D_{kj}\left(\alpha^2 L_{kj}^2 - 1\right)} e^{-\alpha z}] \cos C_k x \cos C_j y \quad (25)$$

From this expression, we simulate the excess minority carrier density profile as a function of base depth(z) and magnetic field B as shown in Figure II-6.

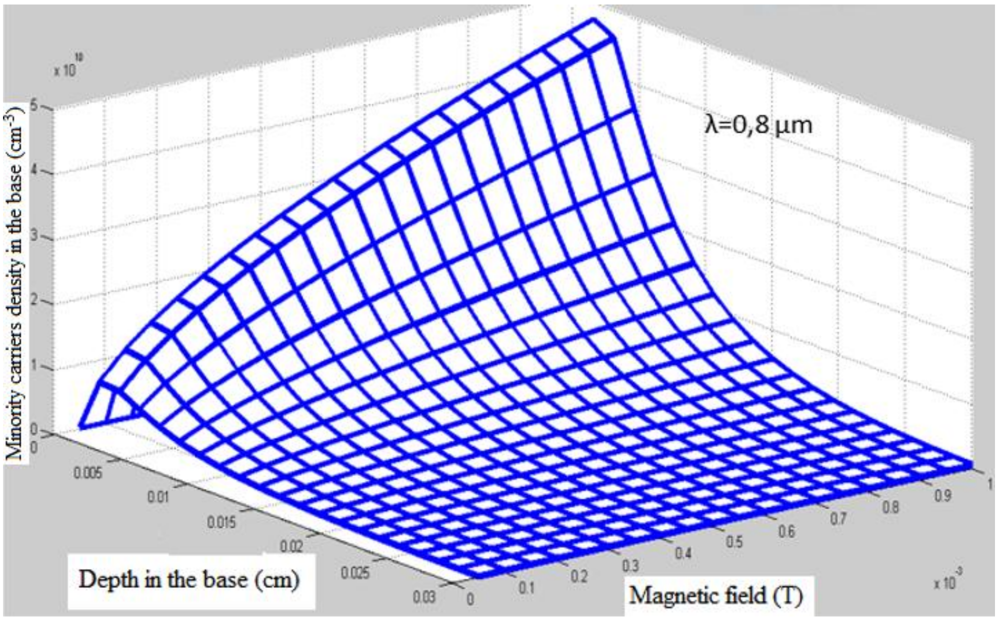

Figure 6: Minority carrier density versus base depth and magnetic field
(Sf = 5.10^3 cm.s^{-1}, Sb = 5.10^3 cm.s^{-1}) Sg=5.10^2 cm.s^{-1}; g_x=g_y= 0.05 cm; x=y=0.

We note that for a given magnetic field value, the profile of the excess minority carrier density as a function of the base depth essentially reveals three zones:

An area near the junction gives a positive density gradient. In this zone of high excess minority density, photogenerated carrier have sufficient energy to cross the junction and contribute to the photocurrent.

A wider area appears, where the excess carrier density gradient is negative; the carrier there, do not have enough energy to cross the junction and participate in the photocurrent. They disappear in the base by recombination in the bulk and at the back surface [20].

These two zones are separated by the points where the gradient of the excess minority density remained zero, therefore the density of charge carrier is constant.

Also, we observe a considerable increase in the charge carrier density near the junction (Sf = $5.10^3 m.s^{-1}$) as the magnetic field increases. This is since the charge carrier are deviated from their initial trajectory causing the blocking of, some of them (Lorentz's effect).

2.5.1. Excess minority carrier density in the base: influence the wavelength

The figure 6 and 7 produce excess minority carrier density profiles in the base for short wavelengths λ=0.6µm and λ=0.4µm.

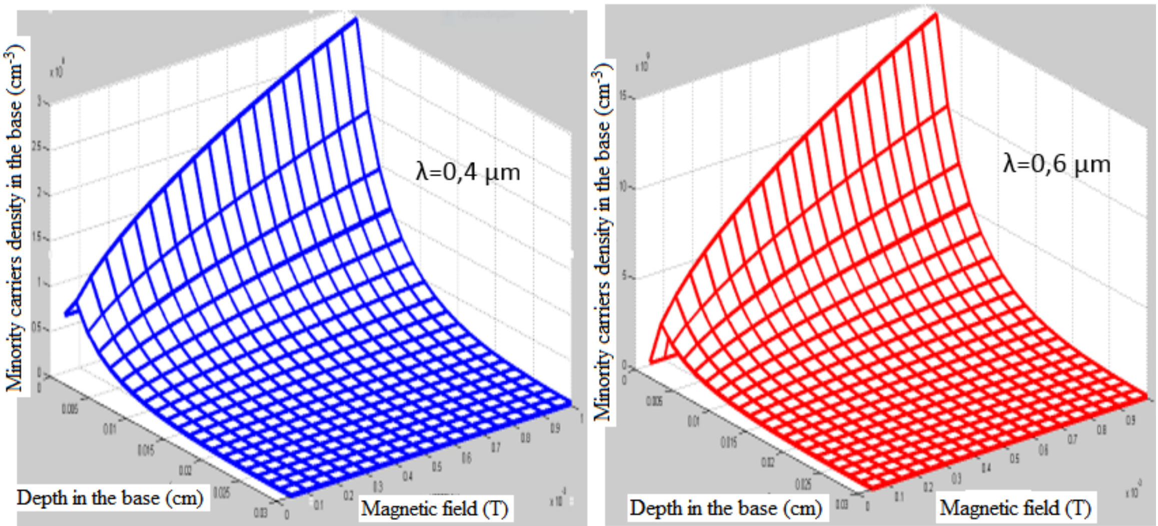

Figure 7: Minority carrier density versus base depth and magnetic field for λ=0.4µm and λ=0.6µm Sf = $5.10^3 cm.s^{-1}$, Sb = $5.10^3 cm.s^{-1}$

We notice that for short wavelength illumination,the excess minority carrierdensity in the base decreases. In Figure II-7 the area where the charge carrier concentration is constant disappears, so the area near the junction where the gradient of the density is positive decreases. This means that the excess minoritycarrier, that can cross the junction and participate in the production of electric current decreases. Therefore, the short wavelengths have a significant influence on the conductivity of the solar cells [45].

2.5.2. Excess minority carrier density in the base: influence the grain boundaries

The density profile of the excess charge carrier as a function of the base depth and the magnetic field for different grain size values is given in the (Figure 8).

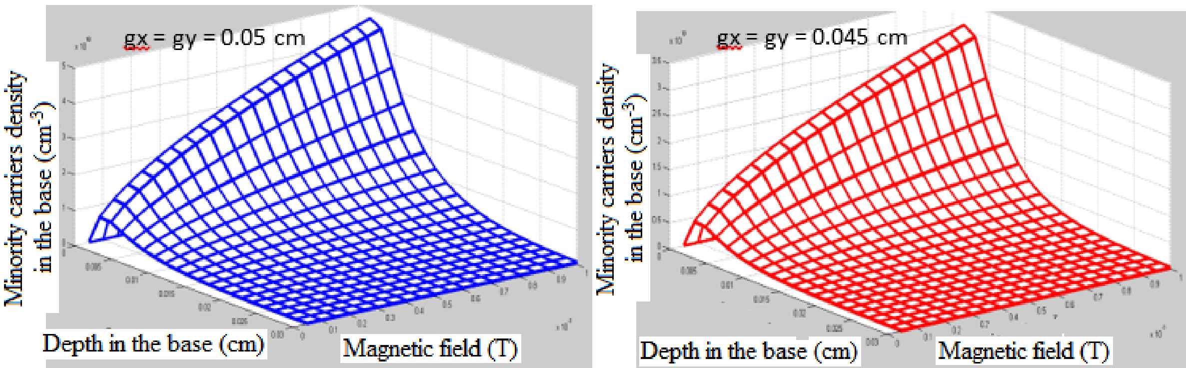

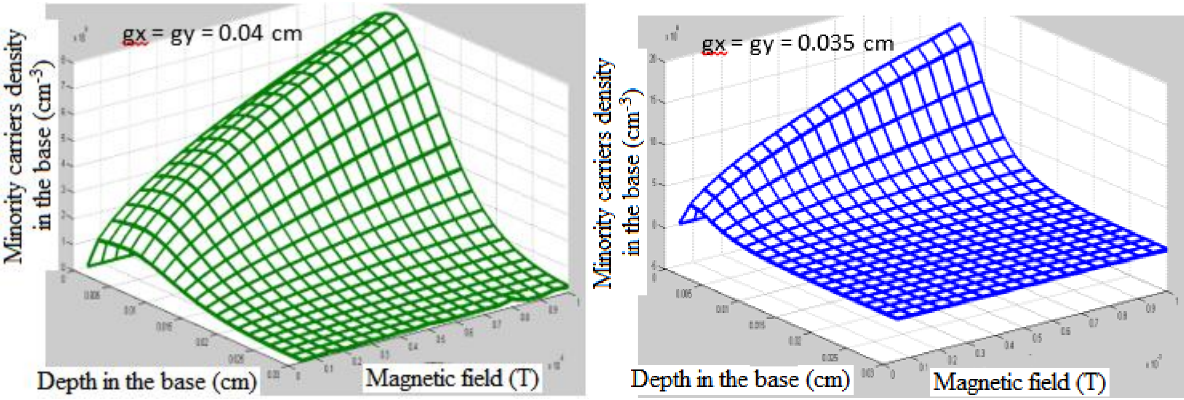

Figure 8: Minority carrier density versus depth in the base and magnetic field for different values the grain boundaries. $Sf = 5.10^3 cm.s^{-1}$, $Sb = 5.10^3 cm.s^{-1}$

The comparative study of the curves in Figure II-8 shows that the smaller the grain size, the lower the density of the excess carrier in the base decreases. All areas shrink; and we find that for gx = gy = 0.035 cm, the recombination of the charge carrieris very important in the bulk.

This phenomenon is explained by the fact that when the grain size is large, recombination rate in the bulk remained less, whatever the grain surface recombinationTherefore, solar cells with large grains are better(large Leff and low Cj values) than those with small grains [34] according to equations (12, 13,15).

3. Conclusion

We have presented in this paper a 3D theoretical study of the solar cell in static mode under monochromatic illumination. The use of the expression of the charge carrier diffusion coefficient, optimized by the relation between the temperature T_{opt} (B) and the magnetic field B, made it possible to determine the space eigenvalues as a function of the optimal temperature T_{opt}(B) and the magnetic field B. The influence of the magnetic field and the short wavelengths on the density of the minority carrier was also carried out.

References

[1]. H. Ohtsuka, M. Sakamoto, K. Tsutsui and Y. Yazawa, (2000). Bifacial Silicon Solar Cells with 21.3% Front Efficiency and 19.8% Rear Efficiency Prog. Photovolt. Res. Appl.;8; pp.385-90

[2]. Le Quang Nam M. Rodot, (1992). Solar cells with 15.6% efficiency on multicrystalline silicon, using impurity gettering back surface field and emitter passivation. Int. J. Solar Energy, vol. 11, pp. 273-279.

[3]. Martin A. Green, (1984). Solar cell minority carrier lifetime using open-circuit voltage decay. Solar Cells, Vol. 11pp 147-161

[4]. Luque A, Ruiz JM, Cuevas A, Eguren J, Agost MG. (1997). Double side solar cells to improve static concentrator. Proceedings of the 0st European Photovoltaic Solar Energy Conference, Luxembourg, 269-277

[5]. Omar Mbao, Moustapha Thiame, Ibrahima LY, Ibrahima Datta, Marcel S. Douf, Youssou Traore, Mor Ndiaye and Grégoire Sissoko, (December 2016). 3D study of a Polycrystalline Bifacial Silicon Solar Cell, Illuminated Simultaneously by Both Sides: Grain Size and Recombination Velocity Influence. International Journal of Innovative Science, Engineering & Technology, Vol. 3 Issue 12, pp. 152-162

[6]. Moustapha Thiame, Alassane Diene, Boureima Seibou, Cheikh Tidiane. Sarr, Mohamed Lemine Ould Cheikh, Ibrahima Diatta, Mayoro Dieye, Youssou Traore, Gregoire Sissoko, (2017). 3D Study of a Bifacial Polycrystalline Silicon Solar Cell Back Surface Illuminated: Influence of Grain Size and Recombination Velocity. Journal of Scientific and Engineering Research, 4(1):135-145

[7]. Avraham Gover, Paul Strella, (1974). Vertical Multijunction Solar-Cell One-Dimensional Analysis. IEEE Transactions on Electron Devices, Vol.21, N°6, pp351-356.

[8]. Martin A. Green, (March 1995). Silicon Solar cells advanced principles & practice Printed by Bridge printer Pty. Ltd. 29-35 Dunning Avenue, Roseberry, Centre for photovoltaic Devices and systems.

[9]. J. Dugas, (1994). 3D modelling of a reverse cell Made with improved multicrystalline silicon wafers. Solar Energy Materials and Solar Cells 32, pp71-88.
[10]. H. El Ghatani and S. Martinuzzi, (August 1989). Influence of dislocation on electrical properties of large grained polycrystalline silicon cells. I. Model. J. Appl. Phys. 66(4), 15, pp. 1717-1722.
[11]. H. L. Diallo, A. S. Maiga, A. Wereme, G. Sissoko, (2008). New approach of both junction and back surface recombination velocity in a 3D modelling study of a polycrystalline silicon solar cell. Eur. Phys. J. Appl. Phys. 42, 203–211
[12]. Nzonzolo, D. Lilonga-Boyenga, G. Sissoko, (March 2014). Illumination Level Effects on Macroscopic Parameters of a Bifacial Solar Cell. Energy and Power Engineering, 6, 25-36**.**
[13]. Mayoro Dieye, Senghane Mbodji, Martial Zoungrana, Issa Zerbo, Biram Dieng, Gregoire Sissoko, (2015). A 3D modelling of solar cell's electric power under real operating point. World Journal of Condensed Matter Physics, 5, 275-283.
[14]. S. Mbodji, B. Mbow, F. I. Barro and G. Sissoko, (2010). A 3D model for thickness and diffusion capacitance of emitter-base junction in a bifacial polycrystalline solar cell. Global Journal of Pure and Applied Sciences. Vol 16, No.4, pp: 469- 477.
[15]. M.C. Halder and T.R. Williams, (1983). Grain boundary effects in polycrystalline silicon solar cells I: Solution of the three dimensional diffusion equation by the green's function method Solar Cells, Vol. 8, Pp 201-223.
[16]. E. D. Stokes and T. L. Chu (1977). Diffusion Lengths in Solar Cells From Short-Circuit Current Measurements. Applied Physics Letters, Vol. 30, N°8, pp 425-426.
[17]. Konstantinos Misiakos and Dimitris Tsamakis, (1994). Electron and Hole Mobilities in Lightly Doped Silicon. Appl. Phys. Lett. 64(15), pp: 2007-2009
[18]. Mandelis, A. (1989). Coupled ac Photocurrent and Photothermal Reflectance Response Theory of Semiconducting p-n Junctions. Journal of Applied Physics, **66**, pp.5572-5583.
[19]. ND. Thiam, A. Diao, M. Ndiaye, A. Dieng, A. Thiam, M. Sarr, A.S. Maiga, G. Sissoko, (2012). Electric equivalent models of intrinsic recombination velocities of a bifacial silicon solar cell under frequency modulation and magnetic field effect. Research Journal of Applied Sciences, Engineering and Technology Vol. 4, (22): 4646-4655.
[20]. F.I. Barro, A. Seidou Maiga, A. Wereme and G. Sissoko, (2010). Determination of recombination parameters in the base of a bifacial silicon solar cell under constant ultispectral light. Physical & Chemical News, 56, 76-84.
[21]. P. Mialhe, G. Sissoko, F. Pelanchon, and J. M. Salagnon, (1992). Régimes transitoires des photopiles: durée de vie des porteurs et vitesse de recombinaison. J. Phys .III, France 2, 2317-2331.
[22]. Albert Zondervan, Leendert A. Verhoef, and Fredrik A. Lindholm, (1988). Measurement Circuits for Silicon-Diode and Solar Cells Lifetime and Surface Recombination Velocity by Electrical Short-Circuit Current Delay. IEEE Transactions on Electron Devices, Vol. 35, No. 1, pp. 85-88.
[23]. J. E. Mahan and D. L. Barnes, (1981). Depletion Layer Effects in the Open-Circuit Voltage-Decay Lifetime Measurement Solid-State Electronics, Vol. 24, N°10, pp. 989-994.
[24]. Bakary Dit Dembo Sylla, Ibrahima LY, Ousmane Sow, Babou Dione, Youssou Traore, Grégoire Sissoko, (2018) Junction Surface Recombination Concept as Applied to Silicon Solar Cell Maximum Power. Point Determination Using Matlab/Simulink: Effect of Temperature. Journal of Modern Physics, 9, 172-188.
[25]. Amary Thiam, Gokhan Sahin, Mohamed Abderrahim Ould El Moujtaba , Babacar Mbow, Marcel Sitor Diouf, Moussa Ibra Ngom, Grégoire Sissoko, (2015). Incidence angle effect on electrical parameters of a bifacial silicon solar cell illuminated by its rear side in frequency domain. Int. J. Pure Appl. Sci. Technol, Vol. 30 Issue 1, p. 29.
[26]. Ibrahima Diatta, Marcel Sitor Diouf, Moustapha Thiame, Youssou Traore, Ousmane Diasse and Gregoire Sissoko, (2017). Influence of temperature on silicon solar cell shunt resistance under monochromatic illumination. Journal of Scientific and Engineering Research, 4(8):30-39.

[27]. Amadou Diao, Mamadou Wade, Moustapha Thiame, Grégoire Sissoko, (2017). Bifacial Silicon Solar Cell Steady Photoconductivity under Constant Magnetic Field and Junction Recombination Velocity Effects. Journal of Modern Physics, 8, 2200-2208

[28]. Richard Mane, Ibrahima LY, Mamadou Wade, Ibrahima Datta, Marcel S. Diouf, Youssou Traore, Mor Ndiaye, Seni Tamba, Grégoire Sissoko, (2017). Minority Carrier Diffusion Coefficient D*(B, T): Study in Temperature on a Silicon Solar Cell under Magnetic Field. Energy and Power Engineering, 9, 1-10.

[29]. Ibrahima Tall, Boureima Seibou, Mohamed Abderrahim Ould El Moujtaba, Amadou Diao, Mamadou Wade, Grégoire Sissoko. (Jan 2015). Diffusion Coefficient Modeling of a Silicon Solar Cell under Irradiation Effect in Frequency: Electric Equivalent Circuit. International Journal of Engineering Trends and Technology (IJETT) –Vol. 19 No. 2 – pp. 56-61.

[30]. M. M. Deme, S. Mbodji, S. Ndoye, A. Thiam, A. Dieng and G. Sissoko (2010). Influence of illumination incidence angle, grain size and grain boundary recombination velocity on the facial solar cell diffusion capacitance. Revues des Energies Renouvelables, Vol. 13, No.1, pp 109-121

[31]. Ndiaye E.H., Sahin G., Dieng M., Thiam A., Diallo H.L., Ndiaye M., Sissokog. (2015). Study of the Intrinsic Recombination Velocity at the Junction of Silicon Solar under Frequency Modulation and Irradiation. Journal of Applied Mathematics and Physics, 3, 1522-1535.

[32]. S. C. Jain, (1981). Theory of photo induced open circuit voltage decay in a solar cell. Solid-State Electronics, Vol. 24, N^{o}12, pp176-183

[33]. A Dieng, I Zerbo, M Wade, A.S Maiga, G Sissoko (2011). Three-dimensional study of a polycrystalline silicon solar cell: the influence of the applied magnetic field on the electrical parameters. Semicond. Sci. Technol. 26,095023 (9pp)

[34]. M.C. Halder and T.R. Williams (1983). Grain boundary effects in polycrystalline silicon solar cells II: numerical calculation of the limiting parameters and maximum efficiency. Solar Cells, Vol. 8, Pp 201-223.

[35]. H. El Ghitani and S. Martinuzzi, (1989). Influence of dislocations on electrical properties of large grained polycrystalline silicon cells. I. Model. J. Appl. Phys., Vol. 66, N°4. Pp 1717-1722,

[36]. J. Oualid, M. Bonfils, J. P. Crest, G. Mathian, H. Amzil, J. Dugas, M. Zehaf and S. Martinuzzi, (1982). Photocurrent and Diffusion Lengths at the Vicinity of Grain Boundaries (g.b.) in N and P-type Polysilicon. Evaluation of the g.b. Recombination Velocity. Revue Phys. Appl. 17, pp119-124

[37]. Th. Flohr and R. Helbig, (1989). Determination of minority-carrier lifetime and surface recombination velocity by optical-beam-induced-current measurements at different light wavelengths. J. Appl. Phys. 66 (7), pp. 3060-3065.

[38]. Amadou Diao, Ndeye Thiam, Martial Zoungrana, Mor Ndiaye, Gôkhan Sahin, Grégoire Sissoko, (2014). Diffusion coefficient in silicon solar cell with applied magnetic field and under frequency: Electric equivalent circuits. World Journal of Condensed Matter Physics, 4, pp 1-9.

[39]. Peter A. Sandborn, Jack R. East, George I. Haddad, (May 1987). Quasi-two-dimensional modeling of GaAsMesfet's. IEEE Transactions on Electron Devices, Vol. ED-34, N^{o}5, pp: 985-991

[40]. Albert Zondervan, Leenfert Verhoef, Fredrik A. Lindholm, and A. Neugroschel, (1988). Electrical Short-Circuit Current Decay: Practical Utility and Variations the Method. J. Appl. Phys. 63 (11), pp5563-5584

[41]. G. Sissoko, S. Sivoththanam, M. Rodot, P. Mialhe, (October 1992). Constant illumination-induced open circuit voltage decay (CIOCVD) method, as applied to high efficiency Si Solar cells for bulk and back surface characterization. 11th European Photovoltaic Solar Energy Conference and Exhibition, Montreux, Switzerland, pp.352-354.

[42]. G. Sissoko, C. Museruka, A. Correa, I. Gaye, A.L. Ndiaye, (1996). Light Spectral Effect on Recombination Parameters of Silicon Solar Cell', Proceedings of the World Renewable Energy Congress, Denver-USA, Part III, pp.1487- 1490.

[43]. B. H. Rose, H. T. Weaver, (1983). Determination of effective surface recombination velocity and minority-carrier lifetime in high-efficiency Si solar cells. J. Appl. Phys. 54. Pp 238-247

[44]. M. Kunst, A. Sanders, (1992). Transport of excess carrier in silicon wafers. Semicond. Sci. Technol. 7, 51-59 in the UK.
[45]. S.C. Jain, (1983). The effective lifetime in semi crystalline silicon. Solar Cells, Vol. 9, Pp 345-352